EFFECT OF PORE STRUCTURE ON ENERGY BARRIERS AND APPLIED VOLTAGE PROFILES

I. Symmetrical Channels

PETER C. JORDAN
Department of Chemistry, Brandeis University, Waltham, Massachusetts 02254

ABSTRACT This paper presents calculations of the image potential for an ion in an aqueous pore spanning a lipid membrane and for the electric field produced in such a pore when a transmembrane potential is applied. The pore diameter may be variable. As long as the length-to-radius ratio in the narrow portion of a channel is large enough, the image potential for an ion in or near the mouth of a channel is determined by the geometry of the mouth. Within the constriction, the image potential of the ion-pore system may be reasonably approximated by constructing an "equivalent pore" of uniform diameter spanning a somewhat thinner membrane. When a transmembrane potential is applied the electric field within a constricted, constant radius, section of the model pore is constant. If the length-to-radius ratio of the narrow part of the channel is not too large or the channel ensemble has wide mouths, the field extends a significant distance into the aqueous region. The method is used to model features of the gramicidin A channel. The energy barrier for hydration (for exiting the channel) is identified with the activation energy for gramicidin conductance (Bamberg and Läuger, 1974, *Biochim. Biophys. Acta.* 367:127).

INTRODUCTION

It is accepted that electrostatic interactions contribute significantly to the energy barrier for the transport of ions across lipid membranes, even when the effect of specialized molecules such as carriers and pores is taken into account (Parsegian, 1969, 1975; Levitt, 1978; Jordan, 1981, 1982, 1983). All these studies have treated the pore as a cylinder of uniform radius piercing a membrane of constant thickness. This is an oversimplification. Whenever structural information is available, whether it is direct, as in the case of the acetylcholine receptor channel (Kistler and Stroud, 1981; Kistler et al., 1982), or inferential, as in the case of the delayed rectifier K channel (Armstrong, 1975a,b; Hille, 1975) and the maxi-K channel (Miller, 1982; Latorre et al., 1982), the evidence suggests that physiological channels are neither symmetric nor of constant diameter. Even the ideal model channel system, gramicidin A, which is essentially a uniform cylinder (Urry, 1971; Koeppe et al., 1978), can only be described by the primitive model, when the channel length and the membrane thickness are equal. In most cases of biophysical interest there must be some curvature in the pore profile.

This paper treats more realistic model pore geometries. The model describes the pore as being composed of a central section of constant diameter attached to mouths that flare outwards, as illustrated in Fig. 1. Both the radius of the mouth and the length of the central segment are variable. While the mathematical analysis is limited to symmetrical pores, the method can be extended to estimate the properties of pores with unsymmetrical geometries as well (see the following paper). A new computational method, which is a natural extension of the one developed previously (Jordan, 1982), is presented. This technique can be used to compute the electric potential within a pore in response to any electrical source. It is applied to two problems: the image potential of an ion in a pore and the electric field produced when a transmembrane potential is applied.

Even though the calculations presented can remove two significant limitations of earlier work, uniformity and symmetry, the models to be analyzed remain crude approximations. The ensemble is still treated in the two-dielectric approximation. The water bathing the membrane and the water within the pore are assumed to be dielectrically equivalent. This is clearly not correct, since dielectric properties are a reflection of the mean total dipole moment (both permanent and induced). Water within the pore has significantly different surroundings from bulk water; the dielectric consequences are, as yet, unknown. The lipid and the pore former are also described as a single electrical phase, even though pore-forming structures, since they commonly bind their permeant ions, are presumably substantially more polar than the membrane itself. Here at least it is possible to correct for the polarizibility differences.

Even though the electrostatic model, which describes an essentially discrete statistical mechanical problem in a

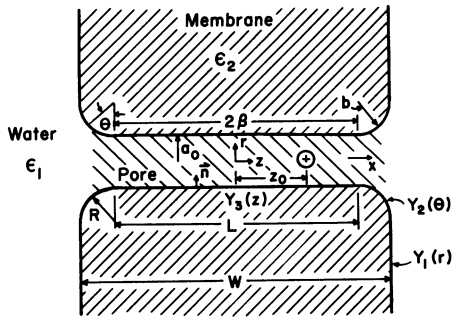

FIGURE 1 Cross section of a cylindrical pore spanning a membrane of dielectric constant ϵ_2. The pore interior and the water are presumed to have the same dielectric constant ϵ_1. The membrane width is W, the constriction length is L, the radius of the mouth opening is R, and the pore radius is a_0. When scaled by the pore radius, the structural parameters describing the model are $\beta = L/2a_0$ and $b = R/a_0$. The distances r, z, and x are scaled by the pore radius; r and z are measured from the center of the pore and x is measured from the entrance to the mouth. The Y_i are scaled surface charge densities in the replacement system and n is the normal pointing outward from the region of dielectric constant ϵ_2.

continuum approximation, is a substantial abstraction, it provides a way to determine the qualitative impact that varying structural features can have on channel conductance. In addition it can be an aid in interpreting experimental results (Jordan, 1983). The calculations outlined in this paper are used to rationalize observations of the effect that lipid variation has on gramicidin conductance (Kolb and Bamberg, 1977).

THEORY

The model being analyzed is illustrated in Fig. 1. A cylindrically symmetric source potential, $V_0(\mathbf{r})$, induces surface charges at the electrical phase boundaries. The resulting electrical potential can be calculated (Levitt, 1978; Jordan, 1982, 1983) by solving a replacement problem in which the system is described as a uniform dielectric with a fictitious surface charge density situated along the phase boundaries. This charge density is chosen to recreate the electric field discontinuity in the real system.

If dimensionless coordinates are used (distance in units of pore radius a_0, potential in units of $e_0/\epsilon_1 a_0$, surface charge density in units of e_0/a_0^2), the equations for the symmetric and antisymmetric contributions to the surface charge density functions, $Y_i^{\pm}$, are found by generalizing my earlier treatment (Jordan, 1982). The result is

$$Y_i^+(t_i) = g\left[F_i^+(t_i) + \sum_{j=1}^{3}\int_{\alpha_j}^{\beta_j}(w_j' dt_j')Q_{ij}^+(t_i; t_j')Y_j^+(t_j')\right] \quad (1)$$

where $g = (K-1)/[2\pi(K+1)]$, $K = \epsilon_1/\epsilon_2$ and

$$t_1 = r, \quad w_1 = r; \qquad \alpha_1 = 1 + b \quad \beta_1 = \infty \quad (2a)$$

$$t_2 = \theta, \quad w_2 = br(\theta) = b[1 + b - b\cos\theta]; \qquad \alpha_2 = 0 \quad \beta_2 = \pi/2 \quad (2b)$$

$$t_3 = z, \quad w_3 = 1; \qquad \alpha_3 = 0 \quad \beta_3 = \delta. \quad (2c)$$

The inhomogeneous terms, F_i, are determined by the gradients of the source potential on the phase boundaries,

$$f_i^{\pm} = \pi\left[(\mathbf{n}_{iR}\cdot\nabla_i V)_R \pm (\mathbf{n}_{iL}\cdot\nabla_i V)_L\right] \quad (3)$$

where $\mathbf{n}_{iR}$ is the outward pointing unit normal to the right-hand branch of surface i, etc. If $i = 2$, $\mathbf{n}_{iR}\cdot\nabla_i = \sin\theta\,(\partial/\partial z) - \cos\theta\,(\partial/\partial r)$ and the right-hand phase boundary is defined by $r = 1 + b - b\cos\theta$, $z = \delta + b\sin\theta$. The kernels can be expressed similarly,

$$Q_{ij}^{\pm} = [\mathbf{n}_{jR}'\cdot\nabla_j' K_0(z_i - z_j', r_i, r_j')]_R \pm [\mathbf{n}_{jL}'\cdot\nabla_j' K_0(z_i - z_j', r_i, r_j')]_L \quad (4)$$

where z_i and r_i are coordinates of the right-hand branch of surface i, $K_0(a,b,c) = 4K(\alpha)/S$, $S = [a^2 + (b+c)^2]^{1/2}$, $\sin\alpha = 2\sqrt{bc}/S$ and $K(\alpha)$ is the complete elliptic integral of the first kind (Abramowitz and Stegun, 1965). Eqs. 3 and 4 are identical to Eqs. 7 and 5 of my earlier paper (Jordan, 1982) on surfaces 1 and 3. The resultant axial electrical potential is

$$\Phi(z) = V_0(z) + \sum_{j=1}^{3}\int_{\alpha_j}^{\beta_j} w_j' dt_j'\,[\theta_j^+(t_j')\,Y_j^+(t_j') + \theta_j^-(t_j')\,Y_j^-(t_j')] \quad (5)$$

$$\theta_j^{\pm} = \tfrac{1}{2}([v_j]_R \pm [v_j]_L),\ v_j = [r_j^2 \pm (z_j - z)^2]^{-1/2}. \quad (6)$$

As there are no sharp corners at which the normal to the electrical phase boundary changes its orientation discontinuously, there are no singularities in the charge density functions Y_i imposed by pore geometry. Singularities, reflecting the properties of the electrical source, are still possible; when they arise, they must be projected out and treated exactly.

In spite of the fact that there are no abrupt changes in $\mathbf{n}$, the solution of Eq. 1 is not straightforward. The kernels, even though no longer singular, are ill defined at the merge points: the widest and narrowest points in the channel mouth. For example, at $t_1 \to 1 + b$ and $t_2' \to \pi/2$, $w_2' Q_{12}$ contains a term $-(bx_2')^2/(x_1 + bx_2')^2$ where $x_2' = \pi/2 - t_2'$ and $x_1 = t_1 - 1 - b$. Depending upon the order in which limits are taken, this term may contribute 0, -1, or any in between value to the integrand. There are similar problems with $w_1' Q_{21}$, $w_2' Q_{32}$, and $w_3' Q_{23}$ at the relevant merge points. While these considerations do not introduce mathematical complications, they do create computational problems because the numerical value of the kernel is ill defined at merge points. To develop a computationally efficient solution procedure, it is necessary to treat the merge points exactly using a projection method modeled after the one devised for handling singularities. Define

$$\mathbf{Y} = \mathbf{W} + \boldsymbol{\Omega}\cdot\mathbf{A} \quad (7)$$

where $W_1(1+b)$, $W_2(\pi/2)$, $W_2(0)$, $W_3(\delta)$ are all constrained to be zero and $\boldsymbol{\Omega}$ is the rectangular matrix

$$\boldsymbol{\Omega} = \begin{pmatrix} H(t_1 - 1 - b) & 0 & 0 & 0 \\ 0 & L(\pi/2 - t_2) & L(t_2) & 0 \\ 0 & 0 & 0 & H(-t_3) \end{pmatrix} \quad (8a)$$

$$H(x) = 1 \quad x < 1, \qquad L(x) = 1 \quad x < \pi/4$$
$$= 0 \quad x > 1 \qquad\qquad = 0 \quad x > \pi/4. \quad (8b)$$

The vector $\mathbf{A}$ represents the values of the Y_i at the respective merge points,

$$A_1 = Y_1(1+b), \quad A_2 = Y_2(\pi/2), \quad A_3 = Y_2(0), A_4 = Y_3(\delta). \quad (9)$$

There are discontinuities in $\mathbf{W}$ at $t_1 = b + 2$, $t_2 = \pi/4$ and $t_3 = \delta - 1$; $\mathbf{Y}$ is, of course, continuous.

It is now possible to reformulate Eq. 1 so that an efficient numerical solution procedure can be devised, regardless of the ambiguities in the kernels near the merge points. Substituting Eq. 7 into Eq. 1 determines

both W and A. The result after substantial matrix algebra, is

$$\mathbf{W}(t) = g[\mathbf{F}(t) + \langle \mathbf{Q}(t, t') \cdot \mathbf{W}(t') \rangle + \mathbf{U}(t) \cdot \mathbf{A}] \quad (10a)$$

$$\mathbf{A} = g(\mathbf{1} - g\mathbf{Z})^{-1} \cdot [\mathbf{\Phi} + \mathbf{\Upsilon}] \quad (10b)$$

with

$$\mathbf{U}(t) = \langle \mathbf{Q}(t, t') \cdot \mathbf{\Omega}(t') \rangle - \mathbf{\Omega}(t)/g \quad (11a)$$

$$\mathbf{\Phi} = \begin{pmatrix} F_1(1+b) \\ F_2(\pi/2) \\ F_2(0) \\ F_3(\delta) \end{pmatrix}, \quad \mathbf{\Upsilon} = \begin{pmatrix} \langle Q_1(1+b, t') \cdot W(t') \rangle \\ \langle Q_2(\pi/2, t') \cdot W(t') \rangle \\ \langle Q_2(0, t') \cdot W(t') \rangle \\ \langle Q_3(\delta, t') \cdot W(t') \rangle \end{pmatrix} \quad (11b)$$

$$\mathbf{Z} = \begin{pmatrix} \langle \mathbf{Q}_1(1+b, t') \cdot \mathbf{\Omega}(t') \rangle \\ \langle \mathbf{Q}_2(\pi/2, t') \cdot \mathbf{\Omega}(t') \rangle \\ \langle \mathbf{Q}_2(0, t') \cdot \mathbf{\Omega}(t') \rangle \\ \langle \mathbf{Q}_3(\delta, t') \cdot \mathbf{\Omega}(t') \rangle \end{pmatrix}. \quad (11c)$$

The notation $\langle\ \rangle$ indicates integration over the variables t_j'. The vectors $\mathbf{Q}_i$ have the components Q_{i1}, Q_{i2}, and Q_{i3}. Written this way, Eq. 10 can be solved rapidly and reliably by iterative numerical methods, among them successive approximations or averaging functional corrections (Luchka, 1965). A possible initial approximation is $\mathbf{A}_0 = g(\mathbf{1} - g\mathbf{Z})^{-1} \cdot \mathbf{\Phi}$, $\mathbf{W}_0(t) = g[\mathbf{F}(t) + \mathbf{U}(t) \cdot \mathbf{A}_0]$. Other initial values are also possible; in any case the basic constraint on W at the merge points must be satisfied at every iterative level.

The analysis requires some elaboration if it is to be used to compute the profile due to an applied potential. The inhomogeneous terms can be established using arguments given previously (Levitt, 1978; Jordan, 1982). Only the F_i^- are nonzero. Because the electrical phase boundary is curved and the thickness of the membranelike region is variable, some care is required in determining F_2^-. If it is assumed that altering the membrane thickness alters the local capacitance, the F_2^-/F_1^- ratio is

$$F_2^-/F_1^- = \delta \cos\theta/\delta(\theta), \delta(\theta) = \beta + b(1 - \sin\theta); \quad (12a)$$

if local capacitance effects are ignored this ratio is simply

$$F_2^-/F_1^- = \cos\theta. \quad (12b)$$

In either case F_3^- is zero. The approach presented previously (Jordan, 1982) can then be modified and analogues to Eq. 10 constructed.

The numerical solution of Eq. 10 is computationally quite efficient. The grid spacings that were used previously (Jordan, 1982) are adequate for approximating Y_1 and Y_3. The larger the value of b, the more points are needed to establish Y_2. If accuracy of <1% is wanted, Y_2 must be estimated at 20 points along the arc when $b = 10$. Changing the radius requires no change in the spacing of the points; the number required is proportional to the radius of the arc.

RESULTS AND DISCUSSION

The method I have outlined can be used to determine the effect that variation of channel shape, mouth architecture and membrane thickness have on both the image potential and the electric field produced by an applied potential.

Image Potential

Fig. 2 illustrates the image potential, $\Phi(\beta, b)$ for an ion at the center of the model channel depicted in Fig. 1 as a function of channel length to pore diameter ratio, $\beta = L/2a_0$, for a number of channel mouth opening sizes, defined in terms of the parameter $b = R/a_0$. The dielectric ratio is that of the lipid-water system, $K = 40$ ($\epsilon_1 = 80$, $\epsilon_2 = 2$). At larger values of β and b, the curves appear to be converging toward a limit, the value of which should be

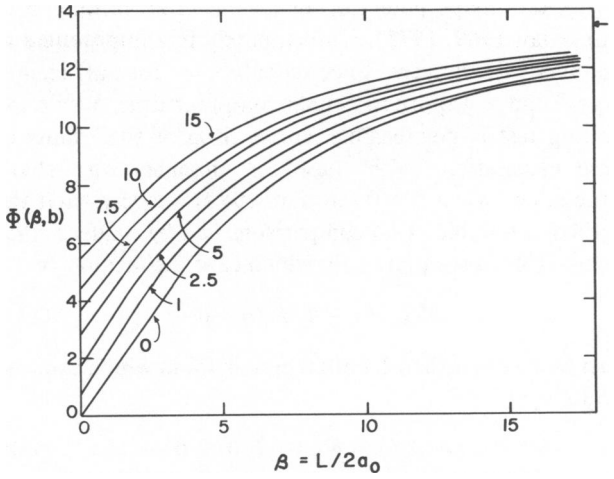

FIGURE 2 Image potential $\Phi(\beta, b)$, in units of $e/\epsilon_1 a_0$, for an ion at the center of a cylindrical channel with the geometry illustrated in Fig. 1. The dielectric ratio, $K = \epsilon_1/\epsilon_2$, is 40. The parameter β is the ratio of the length of the constriction L to its diameter, $2a_0$; b describes the size of the mouth, $b = R/a_0$. Curves for eight different b values are plotted. The width of the membrane is $W = L + 2R$. In these units the potential in an infinite channel (denoted by the arrow) is 13.584. The lines are curves drawn through points calculated using Eq. 5.

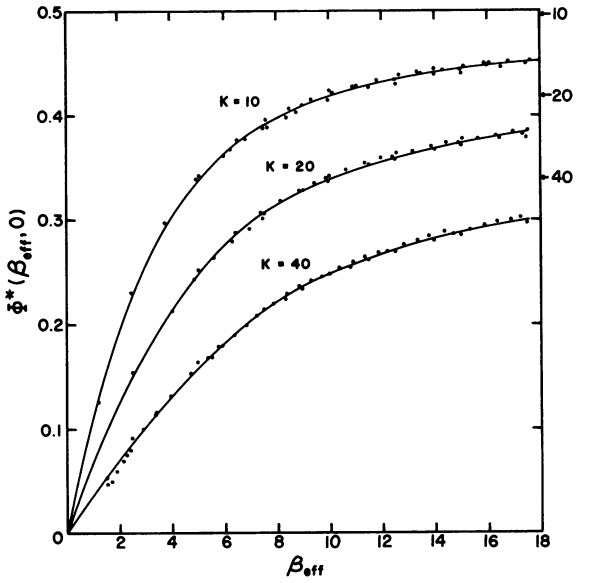

FIGURE 3 Image potential $\Phi^*(\beta_{eff}, 0)$, in units of $e/\epsilon_2 a_0$, for an ion at the center of a cylindrical channel with the geometry illustrated in Fig. 1. The relationship between Φ and Φ^* is $\Phi^* = \Phi/K$. The parameter β_{eff} is defined in the text, Eq. 14. For a given dielectric ratio K, all data fall on the same curve, regardless of the values of β and b. The points were calculated using Eq. 5; the curves were fitted visually. The potentials for infinite channels are indicated by the arrows.

$\Phi_\infty(K)$, the image potential for an ion in an infinite pore (Parsegian 1969, 1975). Unfortunately it is impractical to establish this directly, since calculations, for sufficiently large β and b, require too much computer time. While the limiting test is not feasible, comparison of the results of these calculations with those for channels with sharp corners, i.e., when $b = 0$ (Jordan, 1982) indicates that the method is reliable. Two comparisons can be made. Either shrink W until it equals L, in which case the inequality

$$\Phi(\beta, b) - \Phi(\beta, 0) > 0 \tag{13a}$$

must hold or lengthen L until it equals W, in which case the inequality

$$\Phi(\beta, b) - \Phi(\beta + b, 0) < 0 \tag{13b}$$

must be obeyed. These inequalities are satisfied for all values of β, b, and K for which the image potential was calculated. Values of b as small as 0.5 were used and the differences (Eq. 13) decreased uniformly as $b \rightarrow 0$ for all β's tested.

The curves for different b values are translated from one another by nearly constant amounts. This is demonstrated in Fig. 3 where the data in constructing the curves of Fig. 2 are replotted as a function of an "effective pore length," $\beta_{eff} = \beta + 0.85b^{0.6}$. The result is a general functional form $\Phi(\beta_{eff})$. The curve is essentially $\Phi(\beta_{eff}, 0)$, the peak in the image potential for a right circular cylindrical pore of length to diameter ratio β_{eff}. A similar observation holds for other values of K; data for $K = 20$ and 10 are also included in Fig. 3. In each case, there is a general expression relating Φ and β_{eff} (different for each K); the difference between β_{eff} and β is also dependent on K. For ease of display the function plotted is $\Phi^*(\beta_{eff}) = \Phi(\beta_{eff})/K$. The effective pore length is well represented by the empirical expression

$$\beta_{eff} = \beta + (0.584 + 0.7213 \ln K)\, b^{(1.026 - 0.1154 \ln K)}. \tag{14}$$

Exhaustive tests of this relationship were not carried out for other K's. However, with $K = 80$, some studies were made of a few pore geometries corresponding to $\beta_{eff} = 5$, 10, and 15. The difference between $\Phi(\beta, b)$ and $\Phi(\beta_{eff}, 0)$ was never >3%. Thus, combining Eq. 14 with Eq. 25 of my earlier paper (Jordan, 1982), permits rapid and accurate estimation of the peak in the image potential for a large variety of pore geometries and dielectric ratios.

Varying the mouth size while holding the length of the narrow part of the channel constant (as might occur if the channel forming unit were incorporated into membranes of different width) clearly alters the magnitude of the peak in the image potential. Whether this has a discernible effect on channel conductance depends upon the relative importance of the various physical processes controlling open state conductance in a typical channel. Regardless of the details of the channel structure, conduction can be described in terms of the general five-step process, illustrated in Fig. 4, some steps of which may themselves involve intermediate stages: ionic diffusion towards the entrance, dehydration at the channel entrance, translocation through the channel, hydration at the channel exit and ionic diffusion away from the exit. Changing the mouth size alters the shape of the electrical potential as well as its peak value. It thus affects the energetics of dehydration, translocation, or hydration.

Fig. 5*a–d* illustrates how such variation alters the image potential profile for a range of β and b values. The K value is again 40, representative of a lipid-water system. As expected, the wider the membrane, for a channel of fixed structure, the larger the electrostatic contribution to the energy barrier near the entrance to the narrow part of the channel. An alternative interpretation is that if the geometry of the constricted region is invariant, the larger the channel mouth, the larger the electrostatic image barrier near the entrance to the constriction. Fig. 6 depicts the image potential in the vicinity of the entrance to the narrow segment. For the longer, narrower channels ($\beta \gtrsim 5$) the electrical image profile depends only upon the mouth geometry until the ion has penetrated a distance ~2 or 3 times the pore radius into the narrow part of the channel. As long as the ion is within a few a_0 of the channel mouth, the image potential is β independent for $\beta > 10$. Thus the electrostatic contribution to the energy barrier for dehydration is essentially determined by the geometry at the entrance to the narrow part of the channel. Only if a channel is short and stubby, $\beta \lesssim 2.5$, does the image field, created by an ion outside or just inside the channel mouth, extend far enough so that an electrostatic distinction can be made between a finite and an infinite pore.

The effect that channel architecture has on the image

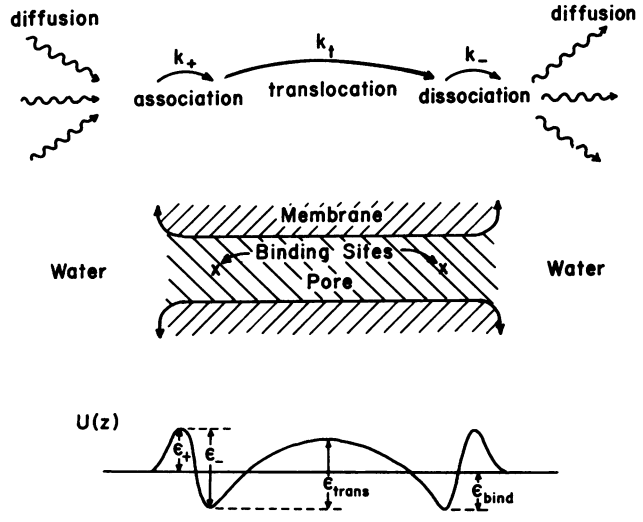

FIGURE 4 Schematic model for ion movement through a symmetrical channel. *Top*: illustration of the five separate steps with their associated rate constants. *Middle:* model of the pore indicating possible location of the binding sites. *Bottom:* potential energy profile with the associated barriers. Local variation in the potential energy has been smoothed.

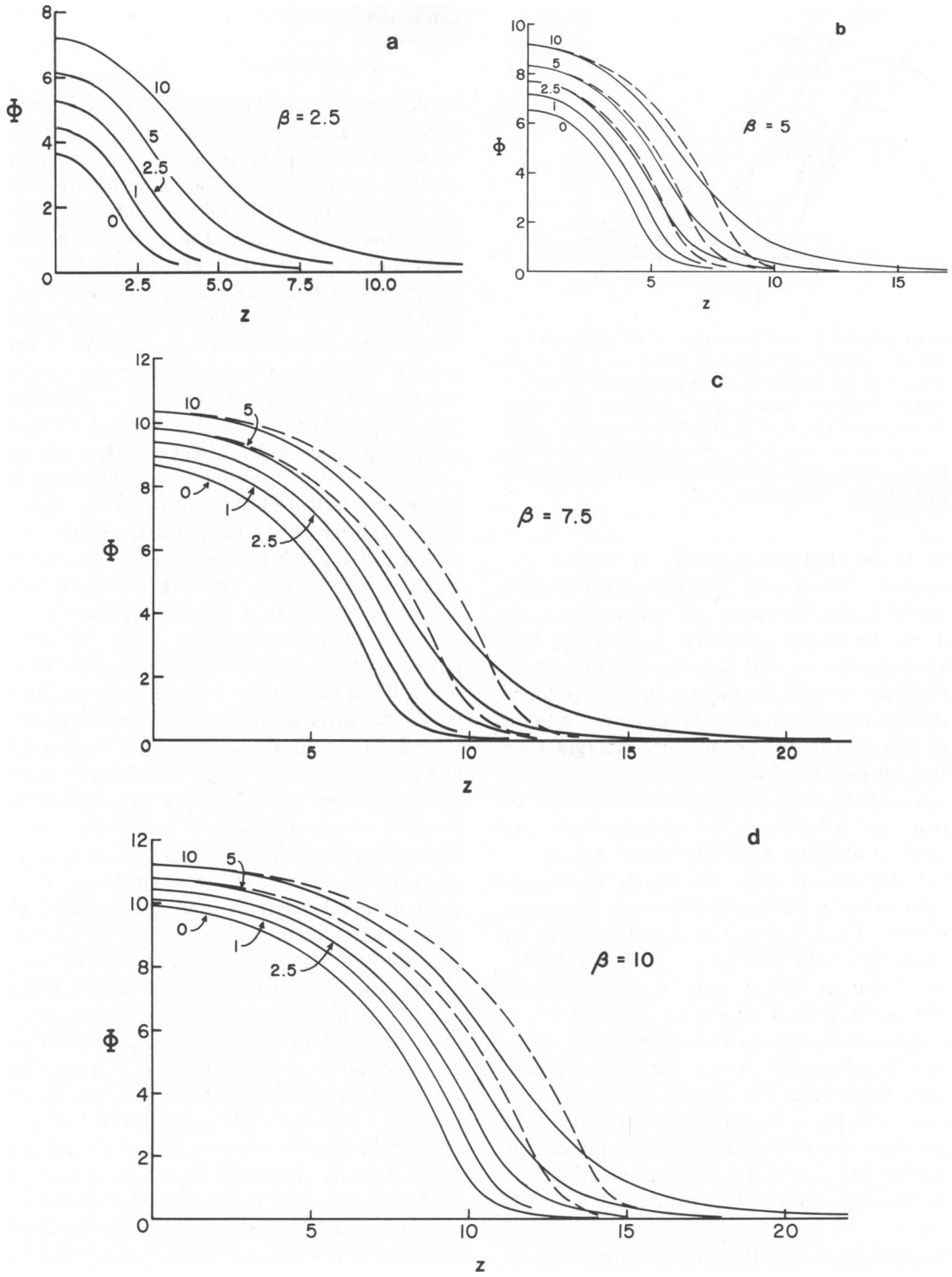

FIGURE 5 Image potential profiles for an ion on the axis of pores with the geometries illustrated in Fig. 1 as a function of the scaled distance z for four values of β. Each set contrasts five different b values. The dashed lines are potentials for uniform pores of length-to-diameter ratio β_{eff}. In these figures the dielectric ratio is 40. The potential is measured in units of $e/\epsilon_1 a_0$.

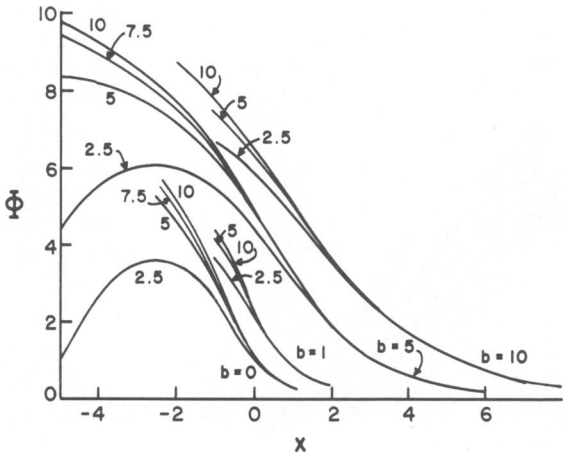

FIGURE 6 Image potential Φ, near the entrance to the constriction for ions on the axis of pores with the geometries illustrated in Fig. 1. The dielectric ratio is 40 and the potential is measured in units of $e/\epsilon_1 a_0$; x is the scaled distance from the channel mouth. Data for four mouth geometries are illustrated ($b = 0$, 1, 5, 10). In each case the image potentials are essentially the same in the region outside the constriction regardless of β. Within the constriction there is no significant difference between the curves for $\beta \geq 5$ as long as $x \gtrsim -2$.

contribution to the electrostatic energy at binding sites near the entrance to the channel mouth is similar. As long as the channel is not too short, all image effects are established by the mouth geometry. Combining these observations demonstrates that it is the structure of the channel mouth that determines the role that image forces have on the binding of ions just inside the entrance to the constriction. The qualitative picture that emerges from Fig. 6 is that, for mouths of similar shape, the larger the mouth region (a) the greater the image contribution to the energy barrier for dehydration and (b) the lower the binding affinity at sites just inside the channel mouth.

The effect that mouth shape has on the barriers to exiting the channel or to translocation through the channel is quite different. From Fig. 5 it is clear that, near the channel mouth, the image field, i.e., $-\partial\Phi/\partial x$, is roughly independent of mouth size as long as β is constant. Restated, the curves Φ (x; β, b) are parallel near $x = \beta$. Thus, the image contributions to the exit barrier, ϵ_- of Fig. 4 are essentially independent of the size of the channel mouths. Again referring to Fig. 5, note that variation of mouth opening size has a less pronounced effect on the image potential near the channel middle than at its mouth. Thus, increasing the size of the channel mouth, for a channel otherwise of fixed structure, reduces the barrier to translocation.

In the channel interior, the effective pore length approximation is useful. I have included, in Figs. 5 *b–d*, the image energy profiles for some "equivalent" uniform cylindrical channels of length to diameter ratio β_{eff}. Even when the real mouth size opening parameter is large ($b = 10$), the image potential in the equivalent pore differs by $< 5\%$ from the exact result as long as the ion has penetrated more than $2a_0$ into the channel. Thus by combining a "mouth potential profile" from Fig. 6 with an "interior potential profile" using β_{eff} a reasonable approximation to the exact result can be determined.

Gramicidin A

To demonstrate the significance of pore shape variation, I have calculated the image energy for a gramicidinlike channel at some special points as a function of membrane width (or mouth radius). The channel is assumed to be 2.6 nm long (Koeppe et al., 1978) with binding sites 0.25 nm from either end (Koeppe et al., 1979). While the electrostatic model of Fig. 1 treats the system as if it were composed of only two dielectric phases, water and lipid, the pore former is in fact a distinguishable electrical domain with an intermediate dielectric constant. A reasonable ϵ value is 4, estimated from measurements on the polypeptide (Gly-Ala) (Tredgold and Hole, 1976) which is analogous to gramicidin A in that none of the amino acids composing the chain has a polar residue. The pore former acts as a dielectric shield; to describe the gramicidin A channel by the two dielectric model of Fig. 1, an "electrical radius" larger than the physical radius of ~0.2 nm (Koeppe et al., 1979) is needed. Calculations on infinitely long channels (Jordan, 1981), show that shielding reduces the image barrier in a system with the electrical cross-section of a gramicidin pore by ~16%. Put differently, the infinite system could be described by the two dielectric model if the radius were increased from its physical value of ~0.2 nm to its equivalent "electrical" value of ~0.25 nm. Choosing this value for a_0, the image energy was calculated at the channel center, at the position of the binding site ($x = +0.25$ nm) and at a point slightly outside the channel entrance where dehydration is probably complete, but solvation by gramicidin is not yet possible ($x = -0.25$ nm). The results are plotted in Fig. 7. The image contribution to the entrance barrier, ϵ_+, and the binding energy, ϵ_{bind}, increase substantially as membrane width increases. However, the exit barrier, ϵ_-, is nearly independent of W and the translocation barrier, ϵ_{trans}, decreases significantly.

These results may help to account for some puzzling observations of the effect that membrane composition has on conductance in single channels of gramicidin A. Kolb and Bamberg (1977), in three sets of measurements using solutions 1 M in Na^+, 1 M in Cs^+, and 0.1 M in Cs^+, found that for membranes between 3.2 and 4.9 nm in width, the single channel conductance in each set varied by a factor of <1.5; in fact, in some cases the conductance was greater in the thicker membranes. Conductances were also deduced from autocorrelation analysis on systems containing many channels. For membranes formed from C_{16}, C_{18}, and C_{20} lipids, the single channel and autocorrelation conductances were the same. For C_{22} lipids, the autocorrelation conductances were, for no clear reason, ~⅓ of the values found in single channel experiments on membranes of the same composition and thickness. However, within the set of C_{22}

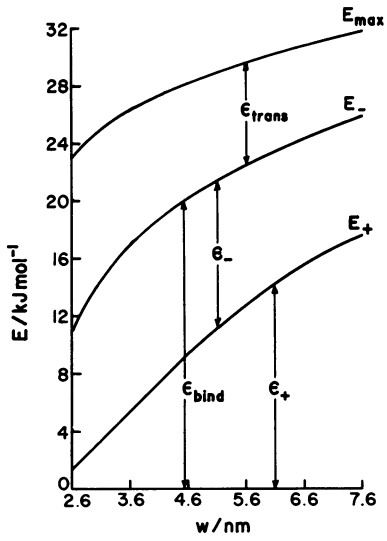

FIGURE 7 Contribution of the ion's electrical image to the total energy of an ion on the axis of a gramicidin-like channel for systems with the geometry illustrated in Fig. 1. The effect that variation of the membrane width, W, has on the energy is plotted for three special points: the center of the channel (E_{max}); the binding site 0.25 nm inside the channel mouth (E_-) and a point 0.25 nm outside the channel mouth, where dehydration is complete but solvation by the pore former is not yet possible (E_+). The quantities ϵ_+, ϵ_{bind}, ϵ_-, and ϵ_{trans} represent the image energy contribution to the dehydration barriers, the binding energy, the dissociation barrier, and the translocation energy, respectively (see Fig. 4).

autocorrelation measurements, conductance appears to be independent of membrane width up to a thickness of ~5.8 nm. Only in the case of single channel measurements on a 6.8 nm membrane formed from a C_{24} lipid is the decrease in conductance clearly related to the bilayer width.

The data indicate that varying bilayer width from 3.2 to 4.9 nm has a negligible effect on the open state conductance. They also suggest that even for a membrane as thick as 5.8 nm, the width may have little influence on the conductance. While there is no compelling reason to believe that gramicidin, when incorporated into thick membranes, would have a structure similar to that illustrated in Fig. 1, such geometries would reduce the local strain in the ensemble due to the difference between the pore length of 2.6 nm and the membrane width. The geometry of Fig. 1 is certainly plausible as long as the membrane does not totally engulf the channel former and effectively seal off the channel mouth. This latter is a distinct possibility if there is a gross structural mismatch such as exists in the 6.8 nm membranes.

From Fig. 7 it is clear that only if conductance is governed by the exit barrier would one expect membrane thickness to insignificantly affect channel conductance. Assuming the structure of Fig. 1, an increase in width from 3.2 to 4.9 nm leads to a decrease in ϵ_- of ~0.6 kJ mol^{-1} and an increase in ϵ_+ of 6.7 kJ mol^{-1}. This thickness change should lead to a slight conductance increase (a factor of ~1.3) if the exit barrier were rate limiting; it should lead to a dramatic conductance drop (a factor of ~15) if the entrance barrier were the major influence. Over the range of membrane thickness, ionic concentrations and applied voltages considered, gramicidin conductance is thus controlled by the exit barrier, a conclusion completely consistent with Andersen's (1983) description of gramicidin conductance. As long as translocation is at least as fast as hydration, which appears to be the case (Andersen and Procopio, 1980), at small-to-intermediate applied potentials, and sufficiently high cation concentrations Andersen's formulation indicates that the ion current is essentially proportional to k_-, the rate of exiting the channel. These are precisely the experimental conditions under which the thickness variation studies were performed (Kolb and Bamberg, 1977), as is necessary if the data are to form a consistent pattern.

If the identification of hydration as the rate-limiting step is correct for the applied potentials, $\lesssim$100 mV, and ionic concentrations, 1 M [Na^+], 0.1 M [Cs^+] and 1 M [Cs^+], used in these experiments, some further observations are possible. Temperature dependent conductance measurements have been made under similar conditions, 1 M in [Na^+] and 135 mV (Bamberg and Läuger, 1974). The apparent activation energy for conduction in lecithin bilayers, ~30 kJ mol^{-1}, must then be identified with ϵ_-, the hydration barrier. Then, using absolute reaction rate theory (see Jordan, 1979), k_- can be estimated as ~2.10^7 s^{-1}. Experimental determinations of k_- have suggested two quite different values, $1.2 \cdot 10^7$ s^{-1} (Andersen and Procopio, 1980) and $2.6 \cdot 10^5$ s^{-1} (Urry et al., 1980); my analysis provides support for the higher value.

Applied Voltage Profiles

Fig. 8, *a–c*, illustrates the potential profile on the channel axis in response to a voltage drop across the membrane for a variety of pore geometries. The length-to-diameter ratios, β, for the constricted region of the channels are 1.25, 2.5, and 5. A β of 1.25 describes a pore with a stubby, short neck; a β of 5 or more is representative of single-file pores. The dielectric ratio for all these calculations is 40. The qualitative structure of the potential profiles is reasonable; as the bilayer width decreases for channels of constant length the curves uniformly approach those determined previously for $W = L$ (Jordan, 1982). As indicated in the theoretical section, there are two reasonable ways to describe the inhomogeneous source term for the curved mouth surface, Eq. 12. The results do not depend upon which choice is made, regardless of channel geometry. The curves are qualitatively quite similar. Over the constricted, constant radius segment of the pore, the electric field is nearly constant. This is true for all values of b and β.

Naturally, as the β/b ratio decreases, the fractional potential drop occurring over the constricted region of the channel decreases as well. For a short constriction in a wide membrane most of the potential drop occurs outside the narrow region. In the most extreme case illustrated, β =

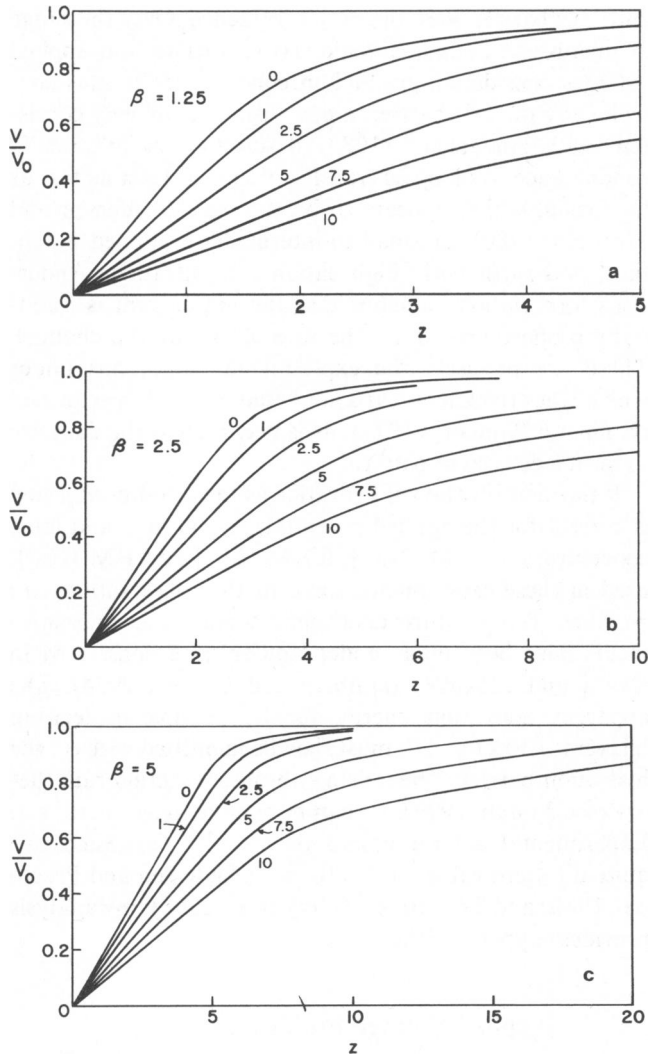

FIGURE 8 Potential profile on the axis of channels with the geometry shown in Fig. 1 for systems with a dielectric ratio of 40. Six mouth size opening parameters, $b = R/a_0$, are contrasted for pores of constant constriction length, $\beta = L/2a_0$. Membrane width is variable, $W = L + 2R$. The total potential change across the membrane is 2 V_0.

1.25 and $b = 10$, only ~17% of the potential drop occurs in the narrow region.

Just as in the case of the image potential, the field external to the constriction is determined by the mouth geometry. This is most easily seen by considering the electrical distance

$$D(z) \equiv [V_0 - V(z)]/2V_0 \qquad (15)$$

which is the fractional potential drop at a point z on the axis; in these calculations the total potential change is $2V_0$. For $z > \beta$, the function $F_D(z) \equiv D(z)/D(\beta)$, plotted in Fig. 9, is essentially independent of β for any given value of b, as long as $\beta \gtrsim 2.5$. Not only is it β independent but the fractional electrical distance function is also only slightly b dependent, if distances are scaled to reflect the differing mouth sizes.

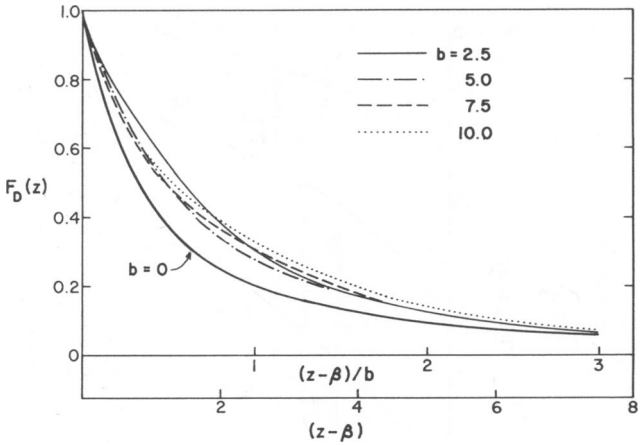

FIGURE 9 Scaled fractional electrical distance function, $F_D(z) = D(z)/D(\beta)$ (see text), as a function of the distance from the entrance to the channel constriction. The geometry is that of Fig. 1; the dielectric ratio is 40. For a given mouth size opening parameter $b = R/a_0$, the results are β (constriction length) independent. For $b \neq 0$, distance is plotted in terms of the scaled quantity $(z - \beta)/b$; for $b = 0$ distance is plotted as $z - \beta$.

The complete potential profile depends upon two quantities, the scaled electrical distance function $F_D(z)$ and the fractional electrical distance to the pore mouth $D(\beta)$. The latter quantity is plotted in Fig. 10 for a variety of pore geometries. It is again apparent that, as long as shielding by the aqueous electrolyte is unimportant, a substantial fraction of the potential drop due to an applied voltage can occur away from the narrowest section of the pore. At ionic strengths of 0.1 M the Debye length is ~1 nm (Wall, 1974); it is ~0.3 nm when the ionic strength is 1 M. Because shielding is essentially complete within two Debye lengths, the field is compressed to within this distance of the membrane surface. As I have pointed out previously (Jordan, 1982), the compression can alter the quantitative details of the potential profile of wide pores or of pores with wide mouths.

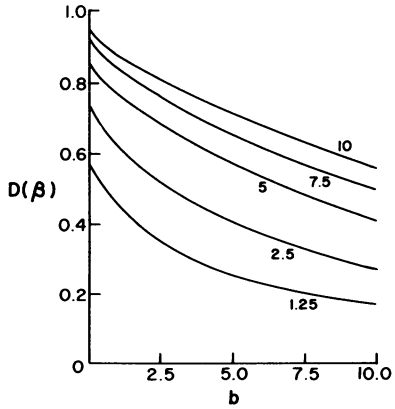

FIGURE 10 Fractional electrical distance to the entrance of the constricted portion of the pore for systems with the geometry illustrated in Fig. 1; the dielectric ratio is 40. Five constriction lengths ($\beta = L/2a_0$) are contrasted for channels with different mouth size opening parameters ($b = R/a_0$).

TABLE I
FRACTIONAL ELECTRICAL DISTANCE TO THE ENTRANCE OF THE CHANNEL AND TO THE ENTRANCE OF THE CONSTRICTED PORTION OF THE CHANNEL FOR PORES OF VARIABLE LENGTH IN A MEMBRANE OF FIXED WIDTH

		Fractional electrical distance to the entrance to the	
		Channel mouth	Constriction
L/nm	*R/nm*		
0.0	2.5	0.145	0.5
1.25	1.875	0.099	0.333
2.5	1.25	0.060	0.215
3.75	0.625	0.043	0.118
5.0	0.0	0.038	0.038

The geometry is illustrated in Fig. 1. The membrane width is 5 nm and the pore diameter is 0.5 nm; the dielectric ratio is 40. The fractional electrical distance to the center of the pore is always 0.5.

To emphasize these points, consider a hypothetical membrane 5.0 nm wide containing a symmetrical pore with a constriction 0.5 nm in diameter. Table I contrasts the fractional electrical distance to the entrance of the channel mouth ($z = \beta + b$ in Fig. 1) and to the entrance of the channel ($z = \beta$ in Fig. 1) for five pores with constricted regions between 0 and 5 nm in length. Electrical distance profiles of the various pores are illustrated in Fig. 11. Changing the mouth size in membranes of constant width substantially changes the relationship between physical and electrical distance, especially at small electrical distances. An electrical distance of 0.1 can be anywhere from ~1.2 nm outside the membrane (when $L = 0$) to ~0.6 nm inside the membrane (when $L = 1.25$ nm). An electrical distance of 0.15 could correspond to a physical distance between 0.1 and 0.96 nm inside the membrane depending on the constriction length. As the field can extend so far beyond the membrane for wide-mouthed pores, electrolyte shielding may be quite important. For the pore with the widest mouth, the radius is so large that shielding is significant at low ionic strengths. For the pore with the fairly small mouth ($L = 3.75$ nm) shielding will still be important at the channel entrance if ionic strength is large enough, since the mouth diameter is equivalent to ~4 Debye lengths when the ionic strength is 1 M. While only an insignificant potential drop can occur in the aqueous region, at all but the very highest ionic strengths (~5 M) shielding does not confine the field to the constriction. A substantial potential change always takes place between the channel entrance and the neck entrance; while this may be reduced by shielding, it is unlikely to be eliminated.

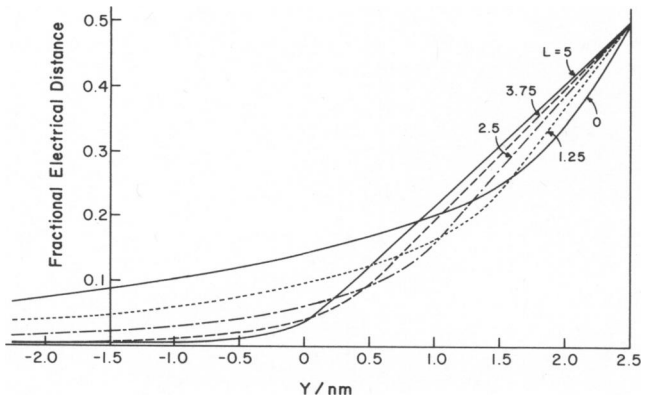

FIGURE 11 Electrical distance profiles for various pores ensembles with the geometry of Fig. 1. The membrane width is 5 nm and the constriction diameter is 0.5 nm; constriction lengths are 0, 1.25, 2.5, 3.75, and 5.0 nm. The distance Y is measured from the membrane-water interface; $Y = 2.5$ nm is the pore center. The dielectric ration is 40.

I wish to thank C. Miller for critical commentary.

This work was partially supported by a grant from The National Institutes of Health, GM-28643.

Received for publication 6 September 1983 and in final form 20 January 1984.

REFERENCES

Abramowitz, M., and I. A. Stegun. 1965. Handbook of Mathematical Functions. Dover Publications Inc., Mineola, NY. 1046 pp.

Andersen, O. S. 1983. Ion movement through gramicidin A channels. Studies on the diffusion-controlled association step. *Biophys. J.* 41:147–165.

Andersen, O. S., and J. Procopio, 1980. Ion movement through gramicidin A channels. On the importance of the aqueous diffusion resistance and ion-water interactions. *Acta Physiol. Scand. Suppl.* 481:27–35.

Armstrong, C. M. 1975*a*. Ionic pores, gates and gating currents. *Q. Rev. Biophys.* 7:179–210.

Armstrong, C. M. 1975*b*. Potassium pores of nerve and muscle membrane. *In* Membranes. A Series of Advances. G. Eisenman, editor. Marcel Dekker, Inc., New York. 3:325–358.

Bamberg, E., and P. Läuger. 1974. Temperature-dependent properties of gramicidin A channels. *Biochem. Biophys. Acta.* 367:127–133.

Hille, B. 1975. Ionic selectivity of Na and K channels of nerve membranes. *In* Membranes. A Series of Advances. G. Eisenman, editor. Marcel Dekker, Inc., New York. 3:255–323.

Jordan, P. C. 1979. Chemical Kinetics and Transport. Plenum Publishing Corp., New York, 293–298.

Jordan, P. C. 1981. Energy barriers for the passage of ions through channels. Exact solution of two electrostatic problems. *Biophys. Chem.* 13:203–212.

Jordan, P. C. 1982. Electrostatic modeling of ion pores. Energy barriers and electric field profiles. *Biophys. J.* 39:157–164.

Jordan, P. C. 1983. Electrostatic modeling of ion pores. II. Effects attributable to the membrane dipole potential. *Biophys. J.* 41:189–195.

Kistler, J., and R. M. Stroud. 1981. Crystalline arrays of membrane-bound acetylcholine receptor. *Proc. Natl. Acad. Sci. USA* 78:3678–3682.

Kistler, J., R. M. Stroud, M. W. Klymkowsky, R. A. Lalancette, and R. H. Fairclough. 1982. Structure and function of an acetycholine receptor. *Biophys. J.* 37:371–383.

Koeppe, R. E., K. O. Hodgson, and L. Stryer. 1978. Helical channels in crystals of gramicidin A and of a cesium-gramicidin A complex: an x-ray diffraction study. *J. Mol. Biol.* 121:41–54.

Koeppe, R. E., J. M. Berg, K. O. Hodgson, and L. Stryer. 1979. Gramicidin A crystals contain two cation binding sites per channel. *Nature (Lond.).* 279:723–725.

Kolb, H. A., and E. Bamberg. 1977. Influence of membrane thickness

and ion concentration on the properties of the gramicidin A channel. Autocorrelation, spectral power density, relaxation and single-channel studies. *Biochim. Biophys. Acta.* 464:127–141.

Latorre, R., C. Vergara, and J. Hidalgo. 1982. Reconstitution in planar lipid bilayers of a Ca^{2+}-dependent K^+ channel from transverse tubule membranes isolated from rabbit skeletal muscle. *Proc. Natl. Acad. Sci. USA.* 79:805–809.

Levitt, D. G. 1978. Electrostatic calculations for an ion channel. I. Energy and potential profiles and interactions between ions. *Biophys. J.* 22:209–219.

Luchka, Y. A. 1965. The Method of Averaging Functional Corrections. Theory and Applications. Academic Press, Inc., New York. 34–52.

Miller, C. 1982. *Bis*-quaternary ammonium blockers as structural probes of the sarcoplasmic reticulum K^+ channel. *J. Gen. Physiol.* 79:869–891.

Parsegian, V. A. 1969. Energy of an ion crossing a low dielectric membrane: solution to four relevant electrostatic problems. *Nature (Lond.).* 221:844–846.

Parsegian, V. A. 1975. Ion-membrane interactions as structural forces. *Ann. NY Acad. Sci.* 264:161–174.

Tredgold, R. H., and P. N. Hole. 1976. Dielectric behaviour of dry synthetic polypeptides. *Biochim. Biophys. Acta.* 443:137–142.

Urry, D. W. 1971. The gramicidin A transmembrane channel: a proposed $\pi_{(L,D)}$ helix. *Proc. Natl. Acad. Sci. USA.* 68:672–676.

Urry, D. W., C. W. Venkatachalam, A. Spisni, P. Läuger, and M. A. Khalid. 1980. Rate theory calculation of gramicidin single channel currents using NMR-derived rate constants. *Proc. Natl. Acad. Sci. USA.* 77:2028–2032.

Wall, F. T. 1974. Chemical Thermodynamics. W. H. Freeman and Co., San Francisco. Third ed. 433–439.